FISEVIER

Contents lists available at ScienceDirect

Chinese Journal of Physics

journal homepage: www.elsevier.com/locate/cjph



An analytical model for the electron effective mobility in a strained silicon inversion layer[☆]



Wang Xiao-Yan*, Xu Xiao-Bo, Wang Hui-Feng

School of Electronic and Control, Chang'an University, Xi'an 710064, China

ARTICLE INFO

Keywords:
Analytical model
Electron mobility
Inversion layer
Quantum confinement
Strain affect,

ABSTRACT

An electron effective mobility analytical model without empirical parameters is investigated for the strained silicon inversion layer, which can be conveniently applied by device and circuit designers. Four kinds of scattering mechanisms, i.e., coulomb scattering, acoustic phonon scattering, intervalley phonon scattering and surface roughness scattering, are taken into account to calculate the electron mobility for the 2D (two-dimensional) inversion layer through a one-dimensional inverse transform. Considering the quantum confinement and strain effect, the valley electron occupancy variation is dissected. In regard to the $\mathrm{Si}/(001)\mathrm{Si}_{1-x}\mathrm{Ge}_x$ and $\mathrm{Si}/(110)\mathrm{Si}_{1-x}\mathrm{Ge}_x$ Si common orientation, the dependence of the electron effective mobility with various Ge content on the inversion charge density is analyzed in detail, and by means of this the mechanism of the mobility enhancement under different situations and the mobility saturation are brought to light.

1. Introduction

Mobility enhancement is an attractive option, because it can potentially improve device performance beyond any of the benefits from device scaling [1]. Strained silicon (S-Si) technology is one of the most advanced technologies in microelectronics, with the advantages of high-mobility, adjustable energy-band structure and compatible processing technology compared with traditional silicon [2]. Carrier mobility with enhancement factor up to 1.8 is achieved for an *n*-channel devices[3]. MOSFET (metal-oxide-semiconductor field-effect transistor) performance improvements are continuing via strained channels, which are being adopted in nearly all 90, 65, and 45 nm logic, communication, and consumer technologies [4]. For high speed and energy efficient applications, Weber et al. presented a 14 nm device platform using strain-engineered FDSOI (fully depleted silicon on insulator) transistors [5]. Intrinsically strained channel techniques are by far the most efficient, with almost 100% of the stress maintained in the channel for long active region length values [6].

Empirical equations for the electron mobility can be used easily for engineering applications, but the physical significance is not clear. A semi-empirical equation is a compromise between easy use and physical significance. Both empirical and semi-empirical methods have parameters which need to be extracted from the actual device. Therefore, their universality are often questioned. The Monte Carlo method, which has a high degree of accuracy, is exploited by researchers to study accurately the inversion electron scattering mechanism. However, this method is too complicated and time consuming, and is hard to embed in the device simulation software, so that it cannot be used in the simulation of the actual circuit. Especially, it is not straightforward for the device and circuit

E-mail address: wxyswallow7907@163.com (W. Xiao-Yan).

^{*} Supported by National Natural Science Foundation of China (Grant no. 61504011), Shaanxi Provincial Natural Science Foundation (Grant no. 2017JQ4025).

^{*} Corresponding author.

designer. The analytical models derived in this paper have the most clear physical significance, which feature simplicity, versatility, and ease of use, so that they can effectively help designers to design, modify and optimize the devices and circuits. The models can also be easily used to calculate the inversion layer electron mobility of an arbitrarily crystal plane with an arbitrarily orientation if the parameters are correctly chosen.

Using the research of mobility on strained Si material for reference, the inversion layer electron effective mobility of biaxial strained Si, by growing a layer of Si on $\mathrm{Si}_{1-x}\mathrm{Ge}_x$, is investigated in this paper. The rest of the paper is organized as follows. Both quantum confinement and the strain effect influence the inversion electron energy, which are the basis of scattering rate models. They are introduced in Section 2. The scattering rates are the key to calculating the mobility according to the mobility formula $\mu = q\tau/m_c$ (m_c indicates the conductive effective mass, and τ indicates the momentum relaxation time, i.e., the reciprocal of the scattering rate). Based on the energy band, the scattering rate models are built in Section 3. Then, the mobility of the common orientations for the common planes (100) and (110) is calculated and simulated in Section 4. Finally, a brief conclusion is drawn in the last section.

2. Quantum confinement and the strain effect

Different from the bulk material, carriers are 2D (two-dimensional) electron/hole gases in the normal inversion operation mode. Two new features must be considered for the carrier transport: 1) electric confinement—also referred to as quantum confinement, and 2) semiconductor-oxide interface scattering, i.e., surface roughness scattering [7].

Due to quantum confinement, the motion of carriers in MOSFET channels is restricted in the gate direction (z direction) and quantized, leaving only a 2D k vector which still characterizes the Bloch wave motion in a plane (x - y plane) normal to the confining potential[7]. An energy band which extends in the k_z direction in bulk materials is now split into a series of subbands. And the six equivalent energy valleys in the bulk materials split into Δ_2 and Δ_4 due to quantum confinement, which reduces the crystal symmetry. The properties of the subbands and transport properties of the inversion and accumulation layers at the semiconductor-insulator interfaces have been reviewed in detail in Ref. [8].

In the triangular potential well approximation, the potential is given by [7]

$$V(z) = \begin{cases} qzE_{\text{eff}} & z > 0, \\ \infty & z \le 0, \end{cases}$$
 (1)

where q stands for the electronic charge and E_{eff} stands for the effective electric field along the z direction. By matching the boundary conditions, the subband energies E_{ni} are [7]

$$E_{\rm ni} = r_{\rm n} \left(\frac{\hbar^2}{2m_{\rm z}}\right)^{1/3} (qE_{\rm eff})^{2/3},\tag{2}$$

where \hbar is Planck's constant over 2π , m_z is the effective mass in the z direction, r_n are the roots for the equation A(-r) = 0: $r_0 = 2.338$, $r_1 = 4.087$, $r_2 = 5.520$, $r_3 = 6.787$, $r_4 = 7.944$, ..., and A(-r) is the Airy function.

At the same time, strain also makes the band structure change. So, for the strained Si inversion layer, the band structure depends on both the quantum confinement and strain splitting. Strain effects in MOSFETs are determined by the coactions of the electric confinement and strain effect. First, quantum confinement and strain splitting can be additive or subtractive. Second, strain alters the in-plane 2D band structures, leading to changes of both the conductivity and density of state (DOS) effective masses [7]. The shift in energies of the conduction band valleys owing to the strain effect can be calculated by deformation potential theory. And the effective mass change owing to the strain effect can be calculated by K·P perturbation theory, which is presented thoroughly in Ref. [9].

3. Scattering models

There are many reasons why the transport properties of the electron gas in a silicon MOS inversion layer should be treated as a two-dimensional electron gas (2DEG) [10], where the motion perpendicular to the surface is quantized, instead of a 3DEG [11], even at room temperature. In the NMOSFET inversion layer, except for ionized impurity scattering, acoustic phonon intravalley scattering and intervalley scattering, surface roughness scattering must be included, as the introduction above said. The various scattering rates based on 2DEG transport theories are as follows:

With respect to the scattering potential, we use a screened coulomb potential function, which is written as the following formula:

$$V(r) = \frac{-q^2}{4\pi\bar{\epsilon}r} \exp(-f_{\rm sc}r),\tag{3}$$

where $\bar{\mathcal{E}}$ is the average permittivity,

$$\bar{\mathcal{E}} = \frac{\mathcal{E}_{\rm si} + \mathcal{E}_{\rm ox}}{2},\tag{4}$$

 \mathcal{E}_{Si} denotes the permittivity of Si and \mathcal{E}_{ox} denotes the permittivity of SiO₂. The screening wave vector, f_{sc} , is given as the inverse of the Debye length for semiconductors [12]:

$$f_{\rm sc} = \sqrt{\frac{q^2 N_{\rm inv}}{\mathcal{E}_{\rm si} Z_{\rm eff}}} K_{\rm B} T, \tag{5}$$

where N_{inv} means the average 2D inversion charge density at any point along the channel of the MOSFET, K_B means Boltzmann's constant, T is the temperature, and Z_{eff} is the average depth of the inversion layer at any point along the channel of the MOSFET, which is expressed by [10]

$$Z_{\rm eff} = Z_{\rm QM} + Z_{\rm CL},\tag{6}$$

where Z_{OM} is given by

$$Z_{\rm QM} = \left(\frac{9\hbar^2}{4m_{\rm z}qE_{\rm eff}}\right)^{1/3},\tag{7}$$

 $Z_{\rm CL}$ is given by

$$Z_{\rm CL} = \frac{3K_{\rm B}T}{2qE_{\rm eff}} \tag{8}$$

and $E_{\rm eff}$ is the effective transverse field defined as [13]

$$E_{\text{eff}} = \frac{q}{\mathcal{E}_{\text{Si}}} (\eta Q_{\text{inv}} + Q_{\text{B}}), \tag{9}$$

where $\eta = 1/2$ for (100) electrons and $\eta = 1/3$ for (110) and (111) electrons, $Q_{\rm inv}$ describes the inversion carrier density, and $Q_{\rm B}$ describes the depleted charge density given by

$$Q_{\rm B} = \left(\frac{4\mathcal{E}_{\rm si}\phi_{\rm B}N_{\rm sub}}{q}\right)^{0.5},\tag{10}$$

$$\phi_{\rm B} = \frac{K_{\rm B}T}{q} \ln \left(\frac{N_{\rm sub}}{n_{\rm i}} \right),\tag{11}$$

where $\phi_{\rm B}$ donates the bulk Fermi potential, $N_{\rm sub}$ donates the substrate impurity concentration and $n_{\rm i}$ the intrinsic carrier concentration.

By taking the one-dimensional inverse transform for the matrix element of the 3D scattering case along the z axis (i.e., perpendicular to the channel direction), the quasi-2D matrix element can be derived as

$$H_{2D} = \int_{-\infty}^{\infty} H_{3D} \exp(iq_z z) dq_z$$

$$= \int_{-\infty}^{\infty} \langle \exp(ik \cdot r) | V(r) | \exp(ik' \cdot r) \exp(iq_z z) \rangle \exp(iq_z z) dq_z,$$
(12)

where k and $k^{'}$ are for the electron wave before scattering and after scattering, respectively, and q_z is the z axis component of the scattering wave vector.

Substituting H_{2D} into the Fermi golden rule, the coulomb scattering rate is derived by [12]

$$S_{\text{cou}} = \frac{q^4 (N_{\text{it}} + N_{\text{ox}})}{16\pi \bar{\mathcal{E}}^2 \hbar K_{\text{B}} T} F,\tag{13}$$

the form factor F is expressed by

$$F = \int_{\alpha=0}^{\pi/2} \left(1 - \frac{f_{\rm sc}^2}{\frac{8m_{\rm d}K_{\rm B}T}{\hbar^2} \sin^2 \alpha + f_{\rm sc}^2} \right) \exp \left[-2z \left(\frac{8m_{\rm d}K_{\rm B}T}{\hbar^2} \sin^2 \alpha + f_{\rm sc}^2 \right)^{0.5} \right] d\alpha, \tag{14}$$

where $m_{\rm d}$ is the density of state (DOS) effective mass given by $\sqrt{m_1m_2}$ (m_1 and m_2 are the principal effective masses of the constantenergy ellipse in the surface). $N_{\rm ox}$ and $N_{\rm it}$ are the fixed oxide charge density and interface state charge of unit area, respectively. $N_{\rm it}$ can be gotten by [14]

$$N_{\rm it} = \int_{E_{\rm i}}^{E_{\rm f}} D_{\rm it}(E) \mathrm{d}E,\tag{15}$$

 $E_{\rm f}$ stands for the Fermi energy level, $E_{\rm i}$ stands for the intrinsic Fermi level and $D_{\rm it}$ is the interface density.

Similarly, the acoustic phonon scattering rate and intervalley scattering rate can be derived, for which the 3D matrix elements are investigated comprehensively in Ref. [15], written by the first author of this paper and others persons. The acoustic phonon scattering rate is derived by

$$S_{\rm ac} = \frac{m_{\rm d} K_{\rm B} T Z_{\rm A}^2}{\hbar^3 \rho U_{\rm l}^2},\tag{16}$$

where $Z_{\rm A}$ indicates the electron deformation constant, $U_{\rm I}$ indicates the phonon velocity in silicon, $\rho = \rho_{\rm bulk} Z_{\rm eff}$, $\rho_{\rm bulk}$ indicates the

mass density of the bulk Si atom.

The intervalley scattering rate can be obtained by

$$S_{\text{int}} = \frac{D_{\text{i}}^2 Z_{\text{fi}} m_{\text{d}}}{2\hbar\rho\hbar\omega_{\text{i}}} \left(N_{\text{i}} + \frac{1}{2} \mp \frac{1}{2} \right) U(E \pm \hbar\omega_{\text{i}} - \Delta E_{\text{fi}}), \tag{17}$$

where D_i symbolizes the deformation potential constant, Z_{fi} symbolizes the number of equivalent valleys, ω_i the angular frequency of the phonon and ΔE_{fi} the energy difference between the initial state and final state. The upper and lower signs refer to the absorption and emission processes, respectively. N_i symbolizes the equivalent phonon number, which obeys Bose-Einstein statistics and is expressed as [16]

$$N_{\rm i} = \frac{1}{\exp\left(\frac{\hbar\omega_{\rm i}}{K_{\rm B}T}\right) - 1}.$$
(18)

The surface roughness scattering rate is calculated by the following formula [13]:

$$S_{\rm sr} = \frac{\pi m_{\rm d} q^2 (\Delta L E_{\rm eff})^2}{\hbar^3 \eta^2},\tag{19}$$

where Δ and L represent the mean asperity height and the correlation length for the surface roughness, respectively.

4. Calculation and simulation results for the electron mobility

4.1. Calculation of the electron mobility

Using Matthiessen's rule, the total mobility can be obtained by [10]

$$\frac{1}{\mu_{\text{total}}} = \frac{1}{\mu_{\text{cou}}} + \frac{1}{\mu_{\text{ac}}} + \frac{1}{\mu_{\text{int}}} + \frac{1}{\mu_{\text{sr}}},\tag{20}$$

where μ_{cou} refers to the mobility due to coulomb scattering, μ_{ac} due to the acoustic phonon scattering, μ_{int} due to intervalley scattering, and μ_{sr} due to interface scattering.

For NMOSFETs on (001) wafer Si, quantum confinement makes the six equal valleys split into four higher Δ_4 valleys (the (100) and (010) valleys) and two lower Δ_2 valleys (the (001) valleys) in line with Eq. (2), and the strain effect strengthens the splitting between the Δ_4 and the Δ_2 valleys. For (110) Si, the splitting is similar, except for the Δ_2 valleys being higher than the Δ_4 valleys. Supposing that the electron concentration is n, the electron mobility at the Δ_2 valleys is μ_{001} , the electron mobility at the Δ_4 valleys are μ_{100} and μ_{010} , respectively, and the electron occupancy at the Δ_2 valleys is p, then the electron occupancy at the Δ_4 valleys is 1-p. Hereafter the current density at the electric field \overrightarrow{E} is

$$J = \frac{1 - p}{2} nq\mu_{100} \vec{E} + \frac{1 - p}{2} nq\mu_{010} \vec{E} + pnq\mu_{001} \vec{E},$$
(21)

along with

$$J = nq\mu \overrightarrow{E}. \tag{22}$$

Comparing Eq. (22) with Eq. (21), we have

$$\mu = \frac{1-p}{2}\mu_{100} + \frac{1-p}{2}\mu_{010} + p\mu_{001}.$$
(23)

From (23), it is observed that the subband electron occupancy has an impact on the mobility. The expression for the subband electron occupancy is

$$p_{\rm ni} = \frac{n_{\rm ni}}{\sum_{total} n_{\rm ni}},\tag{24}$$

where $n_{\rm ni}$ can be calculated by [17]

$$n_{\rm ni} = \frac{2m_{\rm di}k_{\rm B}T}{\pi\hbar^2} F_0 \bigg(\frac{E_{\rm f} - E_{\rm ni}}{k_{\rm B}T}\bigg),\tag{25}$$

where

$$F_0(x) = \ln[1 + \exp(x)].$$
 (26)

4.2. Simulation results

The basic physical parameters are the same as those in Ref. [15]. The effective masses for strained $Si/(001)Si_{1-x}Ge_x$ and strained

 $\text{Si/}(110)\text{Si}_{1-x}\text{Ge}_x$ are from Ref. [9] and [18], respectively. For the coulomb scattering, $N_{\text{ox}} = 1*10^{12} \text{ cm}^{-2}$ [19], D_{it} comes from Ref. [20]. For the acoustic phonon intravalley scattering, $Z_A = 12 \text{ eV}$ [21], and the intervalley scattering, $D_i = 19.2*10^8 \text{ eV}$ [21]. For the surface roughness scattering, $\Delta = 0.185 \text{ nm}$, and L = 1.5 nm [22].

Based on the classic sheet approximation for the inversion layer, the mobility is simulated by Matlab. The mobility for strained Si on the (001) plane $Si_{1-x}Ge_x$ buffer (abbreviated as strained $Si/(001)Si_{1-x}Ge_x$, and the other planes are similar) is shown in Section 4.2.1, and the mobility for strained $Si/(110)Si_{1-x}Ge_x$ is shown in 4.2.2. For all the figures below, x denotes the Ge content, and large x means a large biaxial stress because of the lattice mismatch between Si and $Si_{1-x}Ge_x$. The solid lines with nothing refer to bulk Si, the solid lines with the symbols O refer to O0.1, the symbols O0 refer to O0.2, the symbols O0.3 and the symbols O0.4 refer to O0.4.

4.2.1. Strained $Si/(001)Si_{1-x}Ge_x$ electron mobility

For (001) Si, there are several distinct characters. First, the quantum confinement and strain splitting are additive, and the Δ_2 valleys are the lower valleys. The effective mass of the Δ_2 valleys along the z direction is larger than the one of the Δ_4 valleys, so the Δ_2 valleys have a lower energy, in line with Eq. (2). And the stress also makes the Δ_2 valleys low according to deformation potential theory. So, the majority electrons occupy the Δ_2 valleys. Second, the splitting energy between the Δ_2 and Δ_4 valleys becomes larger with an increase of the biaxial stress or electric field. The large splitting energy results in: 1) more electrons stay in the Δ_2 valleys, and 2) the intervalley scattering rate decreases. Third, the Δ_2 valleys have the same conduction effective mass at the strained plane, and have high mobility due to both a small DOS effective mass and a small conduction effective mass. So, the more electrons occupy the Δ_2 valleys, the higher the mobility according to Eq. (23).

On the basis of Eqs. (24)–(26), the electron occupancy is related to the DOS effective mass and the electron energy level, and the splitting energy between the Δ_2 and Δ_4 valleys has more impact on the occupancy. The effective electric field of the inversion influences the energy level according to Eq. (2), and stress influences both the effective mass and energy level, as was presented in Section 2. On account of the relationships between the splitting energy and the electric field, and between the splitting energy and the biaxial stress, for strained Si/(001)Si_{1-x}Ge_x, the Δ_2 valley electron occupancy increases when the effective field or Ge contents increase, and all the electrons will occupy the δ_2 valleys if the splitting energy is large enough due to high field or stress. These conclusions are displayed in Fig. 1.

Fig. 2 indicates the mobility with various Ge content for the [100] orientation strained $Si/(001)Si_{1-x}Ge_x$. In Fig. 2, the isolated symbols represent the data from Ref. [3], and the symbols \times refer to x=0, the filled symbols \bigcirc refer to x=0.1, and the symbols \diamond refer to x=0.2. The simulation results basically accord with the reference data, but there are two differences between the reference and this paper: 1) the data don't match so well, 2) the mobility has a saturation when the Ge content x>0.2 in the reference, while it doesn't in this paper. With regard to the first difference, it maybe comes from the different parameters for the scattering models. For the second difference, it is because the effective mass doesn't change in the reference. To prove this, the mobility is simulated at the condition that effective mass doesn't change with Ge content, and the results show that the mobility will saturate when $x \ge 0.2$, as Fig. 3 clearly shows. For the inversion layer, the DOS effective mass is 2D, which is different from the 3D DOS effective mass that is almost constant in the material, and it changes with strain. As a result, although the effective mass doesn't change much and all the

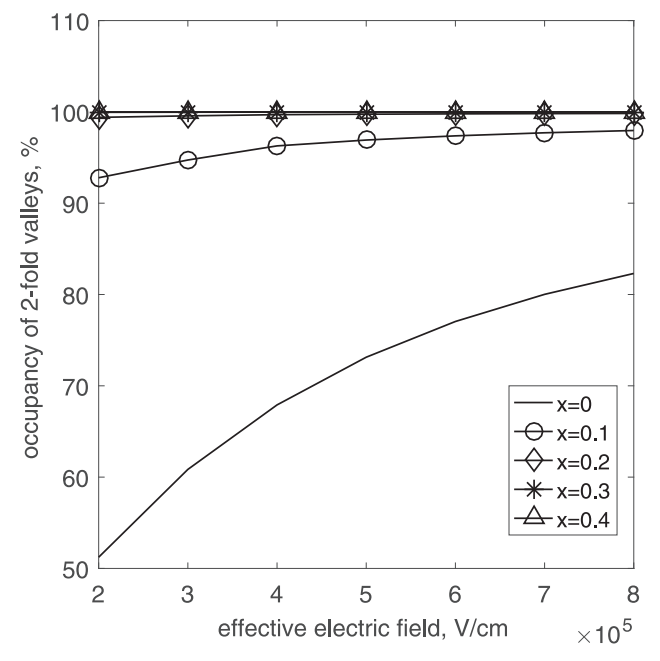


Fig. 1. Occupancy of the strained $Si/(001)Si_{1-x}Ge_x \Delta_2$ valleys.

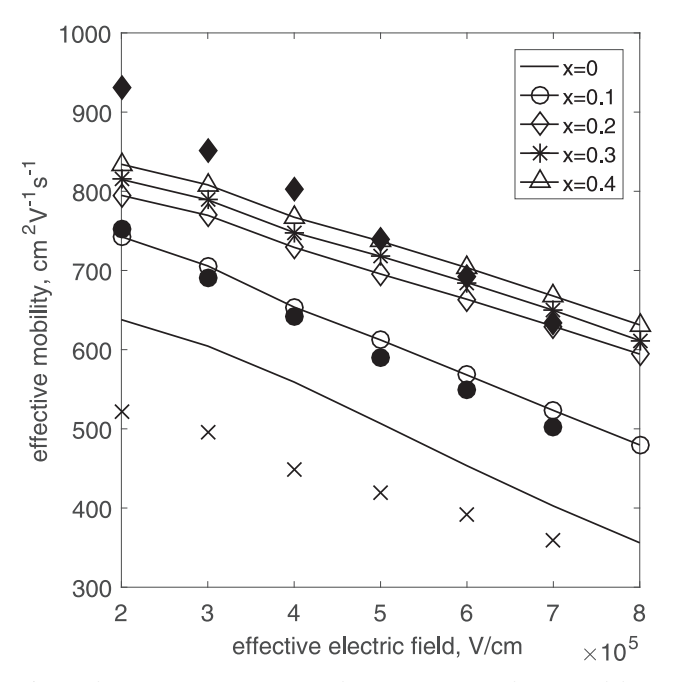


Fig. 2. The [100] orientation strained $Si/(001)Si_{1-x}Ge_x$ electron mobility.

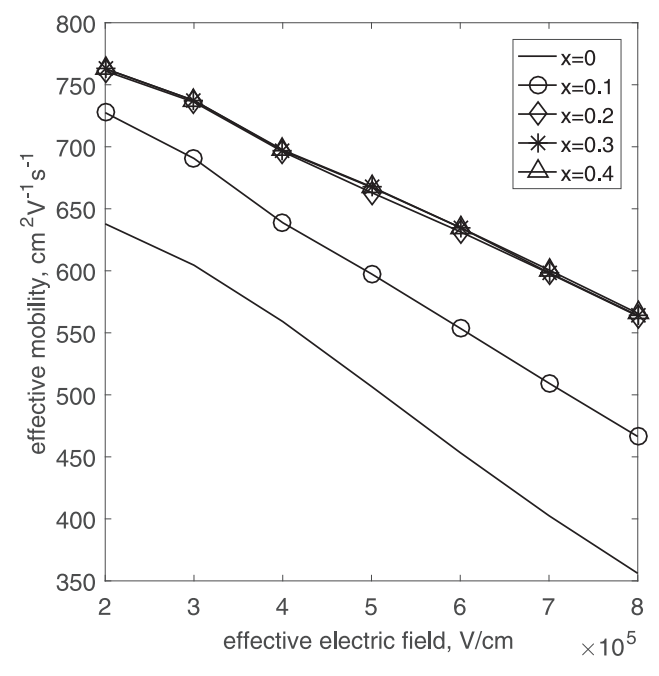


Fig. 3. The [100] strained $Si/(001)Si_{1-x}Ge_x$ electron mobility with unchanged effective mass.

electrons stay at the Δ_2 valleys after the Ge content $x \ge 0.2$, the electron mobility in the inversion layer will not saturate. But if the effective mass remains constant, the mobility will saturate when all the electrons stay in the Δ_2 valleys, as Fig. 3 clearly shows, which means the split energy will not affect the mobility any more.

From Fig. 2 it can be seen that the electron mobility decreases with an increase of the effective electric field, because at low fields the carrier mobility is dominated by coulomb scattering, which is more effectively screened out at higher fields (and thus, higher carrier densities in the inversion layer). At moderate fields, the carrier mobility is determined by the phonon scattering. In the high-field regime, surface roughness scattering dominates the carrier mobility.

In Fig. 2, we can also observe that the electron mobility of [100] orientation strained $Si/(001)Si_{1-x}Ge_x$ increases with an increase of the Ge content. When the Ge content increases the split energy become larger, so that more electrons stay in the Δ_2 valleys, which

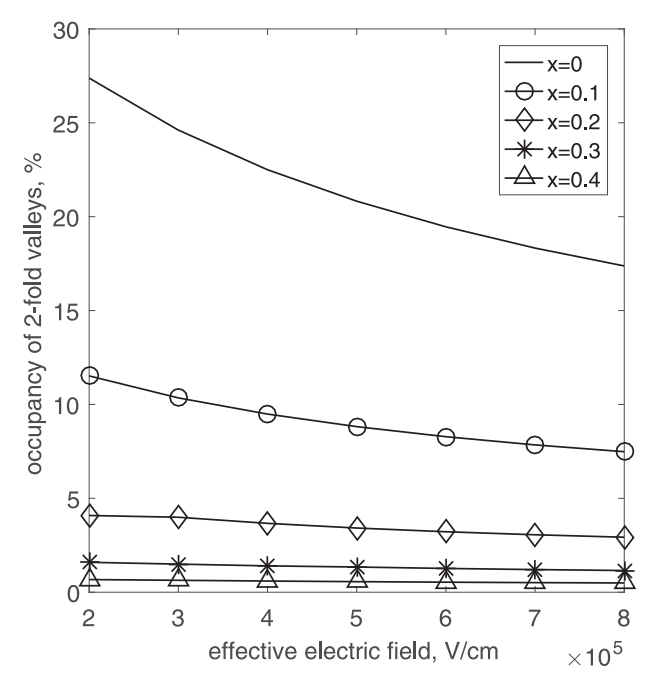


Fig. 4. Occupancy of the strained $Si/(110)Si_{1-x}Ge_x \Delta_2$ valleys.

is conducive to improving mobility, as the beginning of this subsection analyzed.

Regarding the electron mobility of the [110] orientation for strained $Si/(001)Si_{1-x}Ge_x$, the values are same as those of the [100] orientation, because of the identical parameters for all kinds of scattering, the DOS effective mass and the conduction effective mass.

4.2.2. Strained $Si/(110)Si_{1-x}Ge_x$ electron mobility

For (110) Si, it has the same first two characters of (001) Si except that: 1) the Δ_4 valleys are the lower valleys so that a majority of the electrons stay here, and 2) the splitting energy is smaller. The Δ_4 valleys don't have the advantages of the Δ_2 valleys at the (001) plane, having a larger conduction effective mass and a larger DOS effective mass, which results in lower mobility.

As Fig. 4 illustrates, for strained Si/(110)Si_{1-x}Ge_x, a minority of the electrons occupy the Δ_2 valleys, and the occupancy decreases

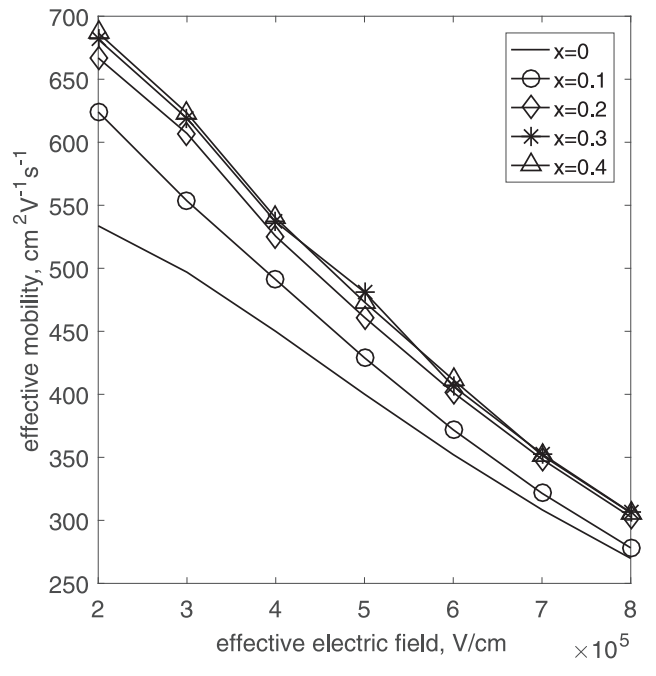


Fig. 5. The [001] orientation strained $Si/(110)Si_{1-x}Ge_x$ electron mobility.

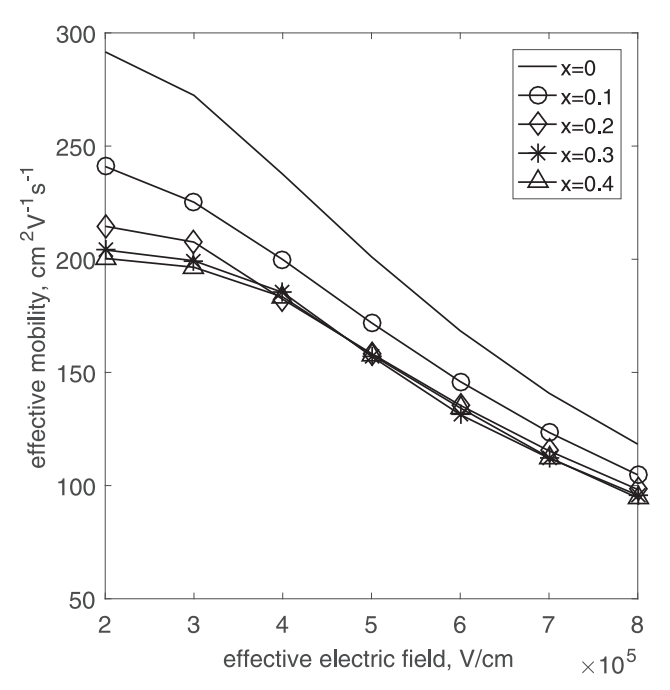


Fig. 6. The [$\bar{1}10$] orientation strained Si/(110)Si_{1-x}Ge_x mobility.

with an increase of the effective electric field and Ge content, which is opposite to that of the (001) plane.

In Fig. 5, the electron mobility of [001] orientation strained $Si/(110)Si_{1-x}Ge_x$ is displayed. Compared with the mobility of strained $Si/(001)Si_{1-x}Ge_x$, the mobility of strained $Si/(110)Si_{1-x}Ge_x$ along the [001] orientation has the same trend on the effective electric field. But the dependence of the mobility on Ge content has two differences. The first, [001] orientation strained $Si/(110)Si_{1-x}Ge_x$ has a smaller mobility, and the reason is that more electrons occupy the Δ_4 valleys. Second, the mobility will saturate when the electrons occupy the Δ_4 valleys totally, because the effective mass of the Δ_4 valleys does not change with Ge content.

The Δ_4 valleys effective mass along the $[\bar{1}10]$ orientation is larger than that of the [001] orientation. So, for the $[\bar{1}10]$ orientation strained $Si/(110)Si_{1-x}Ge_x$, as a result from the larger conduction effective mass, the mobility is lower than that of the [001] orientation, as evidenced in Fig. 6. At the same time, with an increase of stress, more electrons occupy the Δ_4 valleys, which results in lower mobility. In addition, towards the Δ_2 valleys, the effective mass along the $[\bar{1}10]$ orientation increases greatly with increasing Ge content, which lowers the mobility further.

Through the above analysis, it is known that the smaller the 2D DOS effective mass and the smaller the effective mass along the electron moving direction for the valleys in which most of the electrons occupy, the higher the inversion effective electron mobility. So, the mobility of strained $Si/(001)Si_{1-x}Ge_x$ is higher than that of the strained $Si/(110)Si_{1-x}Ge_x$ as Figs. 2, 5 and 6 show. We can expect that the mobility of strained $Si/(111)Si_{1-x}Ge_x$ has lower mobility than strained $Si/(110)Si_{1-x}Ge_x$ due to a larger 2D DOS effective mass.

5. Conclusions

By taking the inverse transform for the matrix element of the 3D scattering case along the z axis, the 2D scattering rate models of the coulomb scattering, acoustic phonon scattering and intervalley scattering are probed. Then, the surface roughness scattering is considered, the effective mobility model for the inversion layer is acquired. The simulation results indicate that strained Si/(001) $Si_{1-x}Ge_x$ has a higher mobility, and the mobility does not saturate on account of the change of the effective mass. The derived mobility model can be employed to design and optimize Si-based MOSFET devices and circuits.

Acknowledgments

We thank the referee for attentive reading and several suggestions that have improved the exposition, and we also thank the language editor and Hsi-Chun Sophie Kao who read the manuscript very carefully and gave us many helpful suggestions.

Supplementary material

Supplementary material associated with this article can be found, in the online version, at doi:10.1016/j.cjph.2018.05.029.

References

- [1] H.H. Liu, X.F. Duan, O. Xu, Finite-element study of strain field in strained-si MOSFET, Micron 40 (2009) 274-278.
- [2] H.Y. Hu, H.M. Zhang, X.Z. Jia, et al., Study on si-sige three-dimensional CMOS integrated circuits, Chin. J. Semicond. 28 (5) (2007) 681–685.
- [3] M.T. Currie, C.W. Leitz, T.A. Langdo, et al., Carrier mobilities and process stability of strained sin- and p-MOSFETs on sige virtual substrates, J. Vac. Sci. Technol. B 19 (2001) 2268–2279.
- [4] X. Chen, S. Fang, W. Gao, et al., Stress proximity technique for performance improvement with dual stress liner at 45nm technology and beyond, Symposium on VLSI Technology, Digest of Technical Papers, 17 (2006), pp. 60–61.
- [5] O. Weber, E. Josse, F. Andrieu, et al., 14 nm FDSOI technology for high speed and energy efficient applications, 2014 Symposium on VLSI technology, (2014), pp. 1–2.
- [6] P. Morin, S. Maitrejean, F. Allibert, et al., A review of the mechanical stressors efficiency applied to the ultra-thin body & buried oxide fully depleted silicon on insulator technology, Solid-State Electron. 117 (2016) 100–116.
- [7] Y. Sun, S.E. Thompson, T. Nishida, Physics of strain effects in semiconductors and metal-oxide-semiconductor field-effect transistors, J. Appl. Phys. 101 (2007).
- [8] T. Ando, A.B. Fowler, F. Stern, Electronic properties of two-dimensional systems, Rev. Mod. Phys. 54 (1982) 437-672.
- [9] S. Richard, N. Cavassilas, F. Aniel, et al., Strained silicon on sige: temperature dependence of carrier effective masses, J. Appl. Phys. 94 (8) (2003) 5088-5094.
- [10] S.A. Schwarz, S.E. Russek, Semi-empirical equations for electron velocity in si: part II-MOS inversion layers, IEEE Trans. Electr. Dev. 30 (12) (1983) 1634–1639.
- [11] T. Nishida, C.T. Sah, A physically based mobility model for MOSFET numerical simulation, IEEE Trans. Electr. Dev. 34 (2) (1987) 310-320.
- [12] S. Potbhare, N. Goldsman, G. Pennington, et al., Characterization of 4h-sic MOSFET interface trap charge density using a first principles coulomb scattering mobility model and device simulation, International Conference on Semiconductor Processes & Devices, (2005), pp. 95–98.
- [13] S. Takagi, A. Touriumi, M. Iwase, et al., On the universality of inversion layer mobility in si MOSFET's: part 11-effects of surface orientation, IEEE Trans. Electr. Dev. 41 (12) (1994) 2363–2368.
- [14] C. Guo, Research on Interface Characteristics of Strained Silicon MOS, Xidian University, 2011. 39-40
- $\textbf{[15]} \hspace{0.2cm} \textbf{X.Y.} \hspace{0.2cm} \textbf{Wang, H.M.} \hspace{0.2cm} \textbf{Zhang, J.J.} \hspace{0.2cm} \textbf{Song, et al., Electron mobility of strained } \textbf{si/(001)} \textbf{si_{1-x}} \textbf{ge_x}, \hspace{0.2cm} \textbf{Acta Physica Sin. 60 (7) (2011). 007205-1-7} \textbf{si_{1-x}} \textbf{ge_{2x}}, \hspace{0.2cm} \textbf{Acta Physica Sin. 60 (7) (2011). 007205-1-7} \textbf{si_{1-x}} \textbf{ge_{2x}}, \hspace{0.2cm} \textbf{Acta Physica Sin. 60 (7) (2011). 007205-1-7} \textbf{si_{1-x}} \textbf{ge_{2x}}, \hspace{0.2cm} \textbf{Acta Physica Sin. 60 (7) (2011). 007205-1-7} \textbf{si_{1-x}} \textbf{ge_{2x}}, \hspace{0.2cm} \textbf{Acta Physica Sin. 60 (7) (2011). 007205-1-7} \textbf{si_{1-x}} \textbf{ge_{2x}}, \hspace{0.2cm} \textbf{Acta Physica Sin. 60 (7) (2011). 007205-1-7} \textbf{si_{1-x}} \textbf{ge_{2x}}, \hspace{0.2cm} \textbf{Acta Physica Sin. 60 (7) (2011). 007205-1-7} \textbf{si_{1-x}} \textbf{ge_{2x}}, \hspace{0.2cm} \textbf{Acta Physica Sin. 60 (7) (2011). 007205-1-7} \textbf{si_{1-x}} \textbf{ge_{2x}}, \hspace{0.2cm} \textbf{Acta Physica Sin. 60 (7) (2011). 007205-1-7} \textbf{si_{1-x}} \textbf{ge_{2x}}, \hspace{0.2cm} \textbf{Acta Physica Sin. 60 (7) (2011). 007205-1-7} \textbf{si_{1-x}} \textbf{ge_{2x}}, \hspace{0.2cm} \textbf{Acta Physica Sin. 60 (7) (2011). 007205-1-7} \textbf{si_{1-x}} \textbf{ge_{2x}}, \hspace{0.2cm} \textbf{Acta Physica Sin. 60 (7) (2011). 007205-1-7} \textbf{si_{1-x}} \textbf{ge_{2x}}, \hspace{0.2cm} \textbf{Acta Physica Sin. 60 (7) (2011). 007205-1-7} \textbf{si_{1-x}} \textbf{ge_{2x}}, \hspace{0.2cm} \textbf{Acta Physica Sin. 60 (7) (2011). 007205-1-7} \textbf{si_{1-x}} \textbf{ge_{2x}}, \hspace{0.2cm} \textbf{Acta Physica Sin. 60 (7) (2011). 007205-1-7} \textbf{ge_{2x}}, \hspace{0.2cm} \textbf{Acta Physica Sin. 60 (7) (2011). 007205-1-7} \textbf{ge_{2x}}, \hspace{0.2cm} \textbf{Acta Physica Sin. 60 (7) (2011). 007205-1-7} \textbf{ge_{2x}}, \hspace{0.2cm} \textbf{Acta Physica Sin. 60 (7) (2011). 007205-1-7} \textbf{ge_{2x}}, \hspace{0.2cm} \textbf{Acta Physica Sin. 60 (7) (2011). 007205-1-7} \textbf{ge_{2x}}, \hspace{0.2cm} \textbf{Acta Physica Sin. 60 (7) (2011). 007205-1-7} \textbf{ge_{2x}}, \hspace{0.2cm} \textbf{Acta Physica Sin. 60 (7) (2011). 007205-1-7} \textbf{ge_{2x}}, \hspace{0.2cm} \textbf{Acta Physica Sin. 60 (7) (2011). 007205-1-7} \textbf{ge_{2x}}, \hspace{0.2cm} \textbf{Acta Physica Sin. 60 (7) (2011). 007205-1-7} \textbf{ge_{2x}}, \hspace{0.2cm} \textbf{Acta Physica Sin. 60 (7) (2011). 007205-1-7} \textbf{ge_{2x}}, \hspace{0.2cm} \textbf{Acta Physica Sin. 60 (7) (2011). 007205-1-7} \textbf{ge_{2x}}, \hspace{0.2cm} \textbf{Act$
- [16] V.A. Vettchinkina, A. Blom, M.A. Odnoblyudov, The monte carlo method applied to carrier transport in si/sige quantum wells, Int. J. Mod. Phys. B 19 (2005) 3353–3377.
- [17] H.C. Moon, S.J. Kim, T.H. Shim, et al., Impact of the top silicon thickness on phonon-limited electron mobility in (110)-oriented ultrathin-body silicon-on-insulator-metal-oxide-semiconductor field-effect transistors, J. Appl. Phys. 102 (2007). 063520-1-5
- [18] M. Bouhassoune, A. Schindlmayr, Ab initio study of strain effects on the quasiparticle bands and effective masses in silicon, Advances in Condensed Matter Physics, (2015), pp. 1–8.
- [19] S. Manzini, Effect of coulomb scattering in n type silicon inversion layers, J. Appl. Phys. 57 (2) (1985) 411–415.
- [20] C. Jungemann, B. Meinerzhagen, M. Eller, On the number of fast interface states of standard CMOS technologies, IEEE Electron. Dev. Lett. 20 (6) (1999) 283–285.
- [21] S. Takagi, J.L. Hoyt, W.J. Jeffrey, et al., Comparative study of phonon-limited mobility of two-dimensional electrons in strained and unstrained si metal-oxide-semiconductor field-effect transistors, J. Appl. Phys. 80 (3) (1996) 1567–1577.
- [22] F. Gámiz, J.B. Roldán, J.E. Carceller, et al., Monte carlo simulation of remote-coulomb-scattering-limited mobility in metal-oxide-semiconductor transistors, Appl. Phys. Lett. 82 (19) (2003) 3251–3253.